Holocene sedimentary history of South Danamandıra Lake: a peatland in west of İstanbul, Çatalca Peninsula, NW Turkey

Özlem MAKAROĞLU[1,*] , **Melda KÜÇÜKDEMİRCİ**[1] , **Nurgül KARLIOĞLU KILIÇ**[2] , **Dursun ACAR**[3] ,
Ali GÜREL[4], **Rüya YILMAZ DAĞDEVİREN**[2] , **Nurettin YAKUPOĞLU**[3] , **Asen SABUNCU**[3] , **Damla ŞAHİN ALTUN**[5] ,
M. Ömer KARAÖZ[5] , **M. Namık ÇAĞATAY**[3]

[1]Department of Geophysical Engineering, İstanbul University-Cerrahpaşa, Büyükçekmece Campus, İstanbul, Turkey
[2]Department of Forest Botany, İstanbul University-Cerrahpaşa, Faculty of Forestry, Bahçeköy Campus, İstanbul, Turkey
[3]EMCOL Research Centre and Geological Engineering Department, Faculty of Mining, İstanbul Technical University, İstanbul, Turkey
[4]Marmara Forestry Research Institute, Fatih Forest Campus, İstanbul, Turkey
[5]Department of Soil Science and Ecology, İstanbul University-Cerrahpaşa, Faculty of Forestry, Bahçeköy Campus, İstanbul, Turkey

Abstract: This study investigates the sedimentological evolution of the South Danamandıra Lake (SDL) lake in Çatalca Peninsula, 70 km west of İstanbul, using Georadar data and multiproxy analyses of five sediment cores. The lake is a 1.3-m deep, endorheic freshwater peatland, heavily colonised by common reed (Phragmites sp.). The multiproxy core investigations include a lithological core description and environmental magnetism, physical properties (gamma density and magnetic susceptibility), geochemical elemental, pollen and radiocarbon dating analyses. The lithological sequence in the lake consists of an upper peat unit and a lower sand-silt-clay unit. The peat unit is characterized by lower magnetic susceptibility, density and lithophile elements (K, Fe, Ti, and Zr) concentrations than the sand-silt-clay unit. Overall interpretation of the multiproxy data and the age-depth model suggest that the SDL was formed in a shallow depression of a fluvial channel at ca 10.9 cal kyr BP, and became a eutrophic lake at 8.1 cal kyr BP during the early Holocene warm period. Redox-sensitive element (i.e. Mn) distribution and mineral magnetic properties indicate that the peat unit has accumulated under anoxic conditions below a thin oxic surficial layer. Increase in the Taraxacum, Asteraceae, and Poaceae pollen percentages, together with high siliciclastic inputs in the lake, indicate that anthropogenic influence in the area started at 5.4 cal kyr BP.

Key words: Danamandıra Lake, Çatalca, Holocene, peatland, environmental magnetism, geochemical properties, geophysical survey

1. Introduction

Peatlands cover only 3% of the world but contain more carbon than the entire forest biomass of the world (Joosten and Clake, 2002). Hence, they are very special ecosystems for their ability to regulate the climate by storing up carbon. They are also important for water purification, flood control, provision of habitat for biodiversity, and for their use as an energy source.

Peatlands are relatively rare in Turkey, with 18 small peatlands covering a total area of 220 km² (Çolak and Günay, 2011; Tanneberger et al., 2017). So far, detailed studies are lacking on sedimentological, hydrological and geochemical evolution of these interesting wetlands in the country. As an initial effort to partially fulfill this gap, we studied sedimentary evolution of the peatland in Danamandıra area of Çatalca Peninsula, located north of the Sea of Marmara (Figure 1). Herewith, we analyzed the morphology and peat-bearing sedimentary infill of

the South Danamandıra Lake (SDL), using bathymetric mapping and subsurface imaging by ground penetrating radar (GPR), GIS-based morphological analysis, and physical, geochemical and radiocarbon dating analyses of sediment cores. This study is a part of an interdisciplinary project that also involves other studies on palynology and chemistry of humic matter composition (Karaöz et al., 2020). The present paper aims to provide the basic geological and sedimentological background for papers which are under preparation within the framework of the project.

The studied Danamandıra peatland (hereafter called South Danamandıra Lake, SDL) is an endorheic (terminal) freshwater lake, presently without an outflow. The lake is colonized mainly by *Carex* sp., *Juncus* sp., *Phragmites* sp., and surrounded by an oak forest. It was declared as a natural conservation area and a first-grade archaeological and cultural site by the Ministry of Culture in 2006. Only a
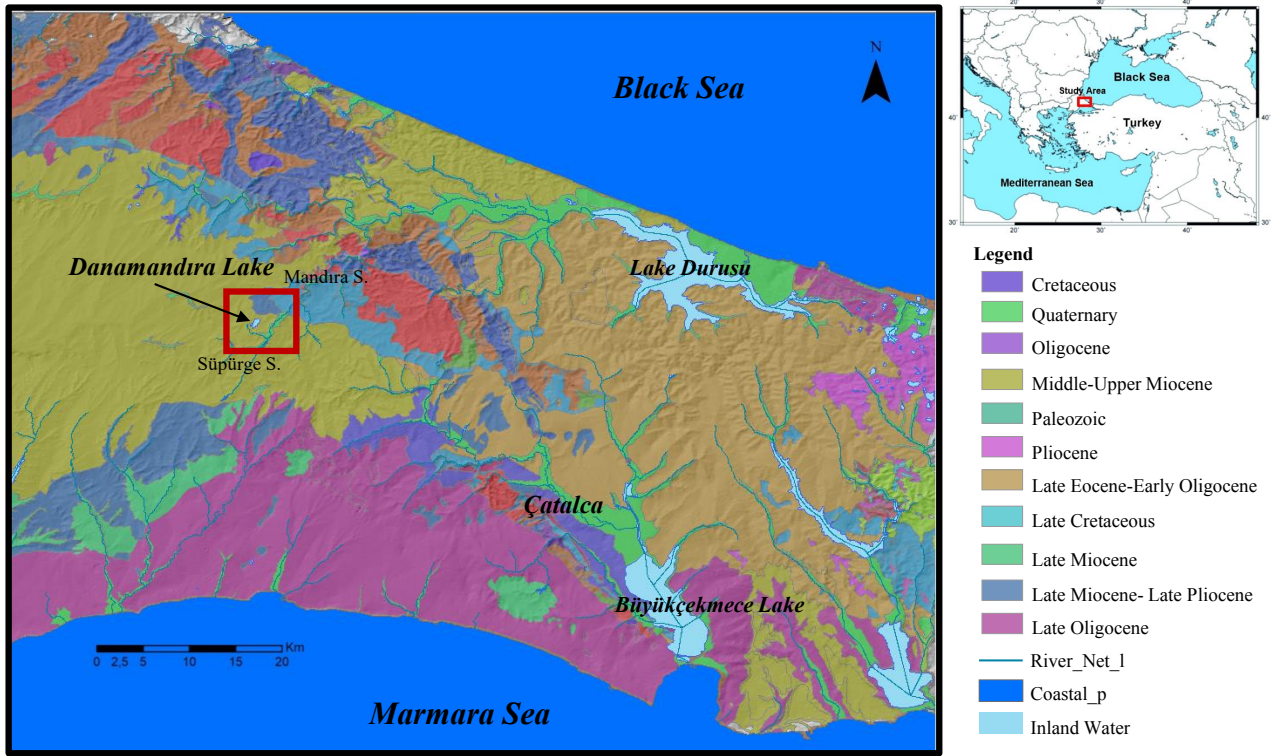
410

Figure 1. Digital Elevation Model (Copernicus Land Monitoring Service, 2020) of the Danamandıra and surrounding area in the Çatalca Peninsula, in NW Turkey, showing the location of Danamandıra (in red frame). Drainage network from EU hydro river network database (EU Copernicus Land Monitoring Service, 2020), which is superimposed on the geology map from Yurtseven and Çağlayan (2002). The drainage network includes Mandıra Stream (Mandıra S.) and Süpürge Stream (Süpürge S.).

few studies about the SDL have been carried out so far. The most important one is the biodiversity study of the wetland, including biology, physiography (morphology, climate) and hydrology of the North and South Danamandıra lakes, by the İstanbul Regional Directorate of Ministry of Forestry and Water Works in 2012 (Republic of Türkiye Ministry of Forestry and Water Affairs, 2012). Albayrak and Özuluğ (2016) performed a taxonomic study of benthic macroinvertebrates and physicochemical analysis of the lake water, while Sevindik et al. (2015) studied freshwater algal flora of the SDL. Other studies focused on seasonal characterization of groundwater properties in Danamandira Village (Acar et al., 2017) and GIS-based digital elevation modeling of the 4th–5th Century AD aqueduct system in the area, which supplied water to the city of Constantinopolis (İstanbul) during the Byzantine times (Ruggeri, 2018; Crapper, 2020).

2. Materials and methods

2.1. Physiographic and geological setting

The SDL is located ca. 70 km west of İstanbul in Çatalca Peninsula (41°17'44.99"N/28°12'55.09"E–41°18'02.23"N/28°13'19.41"E) (Figure 1). Another smaller lake, called the North Danamandıra Lake (NDL),

is located ca. 1.5 km NW of the SDL. The SDL is a small peat-bearing pond with a surface area of 0.295 km². It is elongated in a NE-SW direction, with a maximum length of 1134 m, a width of 410 m, and a maximum depth of 1.3 m (Sevindik et al., 2015) (Figure 2). The NDL is a ca. 0.5 m-deep shallow wetland at ca. 200 masl, and covers a surface area of 0.185 km².

The Danamandıra area is situated in the southern part of the Black Sea drainage basin, close to the drainage divide separating the Black Sea and Sea of Marmara drainage basins. The drainage system around the lakes is a part of a larger network emptying in the Durusu Lake (previously a lagoon) on the Black Sea coast (Republic of Türkiye Ministry of Forestry and Water Affairs, 2012). The network consists of Mandıra Stream and its tributary Süpürge Stream, which are located ca. 400 m east and 150–200 m south and southeast of the lake, respectively. An artificial channel connects the two lakes and transfers the surplus waters of the NDL to the SDL during periods of high precipitation. This study focuses on the much larger SDL (Figure 1).

The SDL basin is a small depression with a submerged lake area of 0.295 km² and drainage area of 0.656 km² (Republic of Türkiye Ministry of Forestry and Water
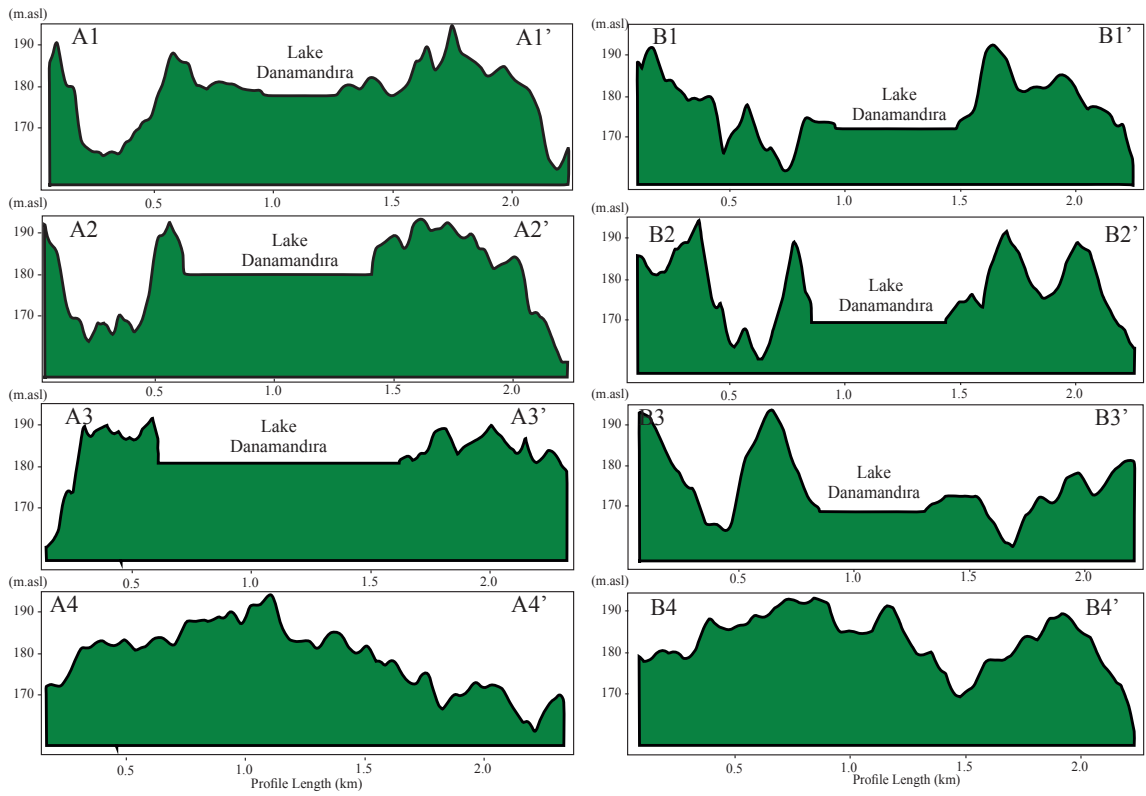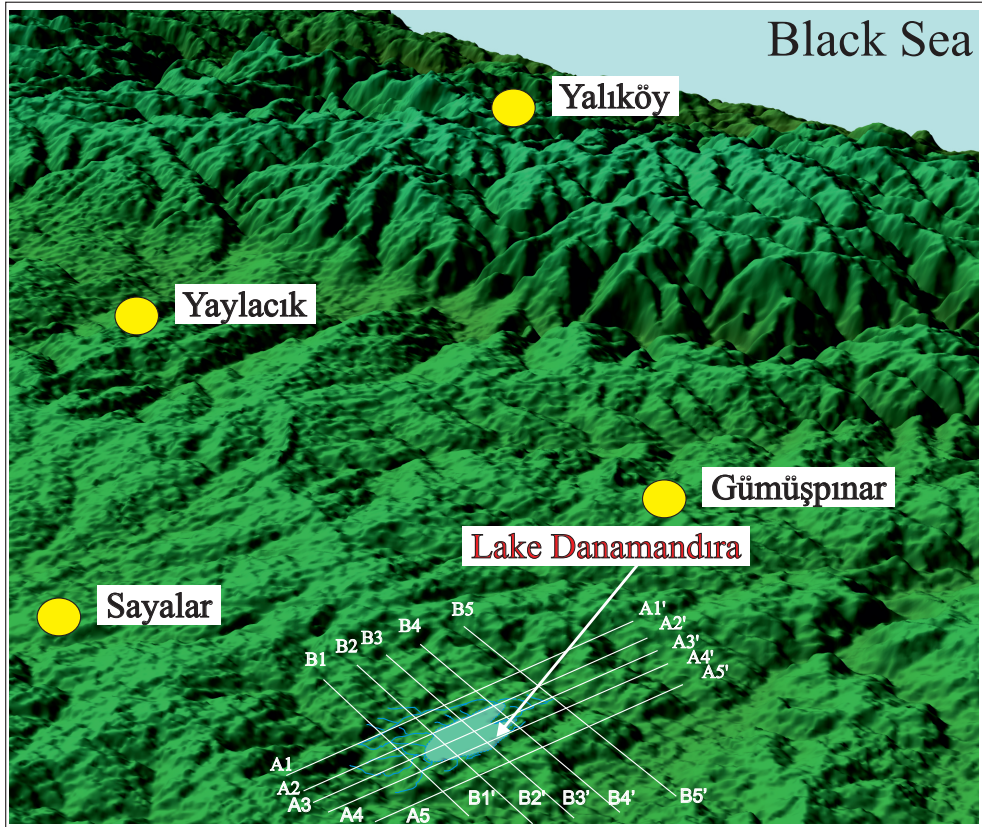
Figure 2. Digitized elevation map and topographic profiles across South Danamandıra Lake and surrounding area, constructed using ASTER satellite imaging (US/Japan ASTER Science Team 2019).

Affairs, 2012). The present lake level stands at 175.5 ± 5.4 masl and the annual lake level variation is ± 0.3 m. The land around the SDL depression has elevations of 2 to 18 m above the lake level. It is connected by artificial canals to the NDL in the north and the Süpürge Stream in the south. The latter canal is presently closed and the lake is a terminal (closed) lake. However, the canal was used during 1990–1995 to completely drain the lake and extract more than 100 truck-loads peat for use as fertilizer. Moreover, the lake might have been in an open mode during the Holocene pluvial periods with its waters outflowing into the Süpürge Stream over a 2–3-m high natural sill located in the artificial canal's location in the southwest (Figure 2). The lake is essentially a freshwater lake with a TDS of 185 mg/L, electrical conductivity (EC) of 168 μS/cm, pH of 7.45 and water clarity (WC) of 4.29 FAU. It contains 17.9 mg/L Ca^{2+}, 20.9 mg/L Mg^{2+}, 15.2 mg/L SO_4^{2-} and 36.86 mg/L Cl.

The Çatalca Peninsula lies mainly within the supra-Mediterranean vegetation belt, with the Euxinian hilly belt to its NW in the Istranca Mountains (Quézel and Médail, 2003). The SDL is surrounded by an oak forest mainly dominated by *Quercus frainetto* Ten. In this forest vegetation, the other main tree species are *Castanea sativa* Mill., *Carpinus orientalis* Mill., *Tilia tomentosa* Moench, *Ostrya carpinifolia* Scop., *Populus tremula* L. and *Pterocarya fraxinifolia* (Lam.) Spach. Also, some meadow grasses (Poaceae) and a small amount of black moss are present in the coastal area of the lake where the forest has been cleared. The SDL is a eutrophic water body, colonized completely by *Phragmites* sp., *Carex* sp., *Juncus* sp. *Iris* sp. and *Nymphea* sp. The water body also contains some phytoplankton and zooplankton taxa (Republic of Türkiye Ministry of Forestry and Water Affairs, 2012). The area around the lake is presently a farmland with large water buffalo and bird populations.

The Çatalca Peninsula is located in a transition area between the Black Sea and Mediterranean climates. The Black Sea climate is observed in the northern parts and the Mediterranean climate in the southern parts of the peninsula. The average annual temperature is 13.7 °C. August is the hottest month with 25.4 °C, and February is the coldest month with 2.8 °C. The average annual precipitation is 563 mm, with the main precipitation occurring as snow and rain during the winter and spring (Doğan, 2011).

The SDL sits over the Middle-Upper Miocene Ergene Formation, which consists of 10 m to 400 m-thick, white to yellowish-white, crossbedded fluvial sandstone and conglomerate with local interbeds of claystone (Yurtseven and Çağlayan, 2002) (Figure 1). This formation overlies a regional unconformity, which is developed by widespread erosion of the Çatalca Peninsula during the Late Oligocene

to Late Miocene, following an uplift event starting in the Early Oligocene (Yılmaz et al., 2009; Okay et al., 2019). In the local area of the lake, the lithology of the Ergene Formation consists of loosely cemented, well sorted, medium- to fine-grained sandstone with silt and clay intercalations. Further north of the Lake Danamandıra, outcrops of yellowish brown loosely cemented conglomerate, coarse sandstone and claystone of the Pliocene Trakya Formation and reefal limestone of the Middle-Upper Eocene Soğucak Formation are present. However, the lake is not affected by any clastic input from these two formations. Carbonate-free, acidic, brown forest soil is the main soil type in the area (Republic of Türkiye Ministry of Forestry and Water Affairs, 2012).

2.2. Ground penetrating radar (GPR)
Ground penetrating radar (GPR) is widely used to probe the shallow subsurface in a broad range of applications in various shallow freshwater environmental settings (Neal, 2004; Butler, 2009; Sambuelli and Bava, 2012). In the SDL, a GPR survey was conducted for bathymetric mapping and determination of shallow stratigraphic architecture. Data were acquired using the GSSI SIR 3000 GPR System of Geophysical Measurements Laboratory at İstanbul University-Cerrahpaşa, which was equipped with a 200-Mhz antenna fixed on the flat base of an inflatable boat. Data along a total 44 profiles measuring 3891 m were collected. All radar reflections within the 180 ns (twt) time window were recorded in the field as 16-bit dynamic range and 512 samples per radar scan. Data processing was done by using GPRSlice V7.0 (Goodman, 2010). Basic data processing as postprocessing pulse regaining was applied to visualize the raw radar pulses and reflections at deeper depths. A band pass filter was applied on radargram to remove undesired frequencies. To remove the background noise, the average pulse (trace) was calculated along each transect, and then subtracted from the recorded pulses along each radargram. Additionally, during the survey, the water temperature was recorded periodically. Using the analysis of the 44 radargrams, the water depth levels were determined and a bathymetry map was generated (Figure 3a). The thickness and approximate volume of the peat in the lake were also determined, using ArcGIS software (Figure 3b).

2.3. Coring and sampling
Coring sites were selected using the GPR bathymetry and subsurface data. A total of 10 cores with a maximum length of 1.52 cm were recovered over a floating platform (4 × 4 m) using a hammer corer. Five representative cores (Kn, Km, Kl, Kj, and K14), located along a NEE-SSW transect parallel to the length of the lake, were used for various analyses (Figure 3a; Table 1). The cores were cut into 1-m sections in the field, and then transported to the core storage repository of the Eastern Mediterranean Centre for Oceanography and Limnology (EMCOL) of İstanbul
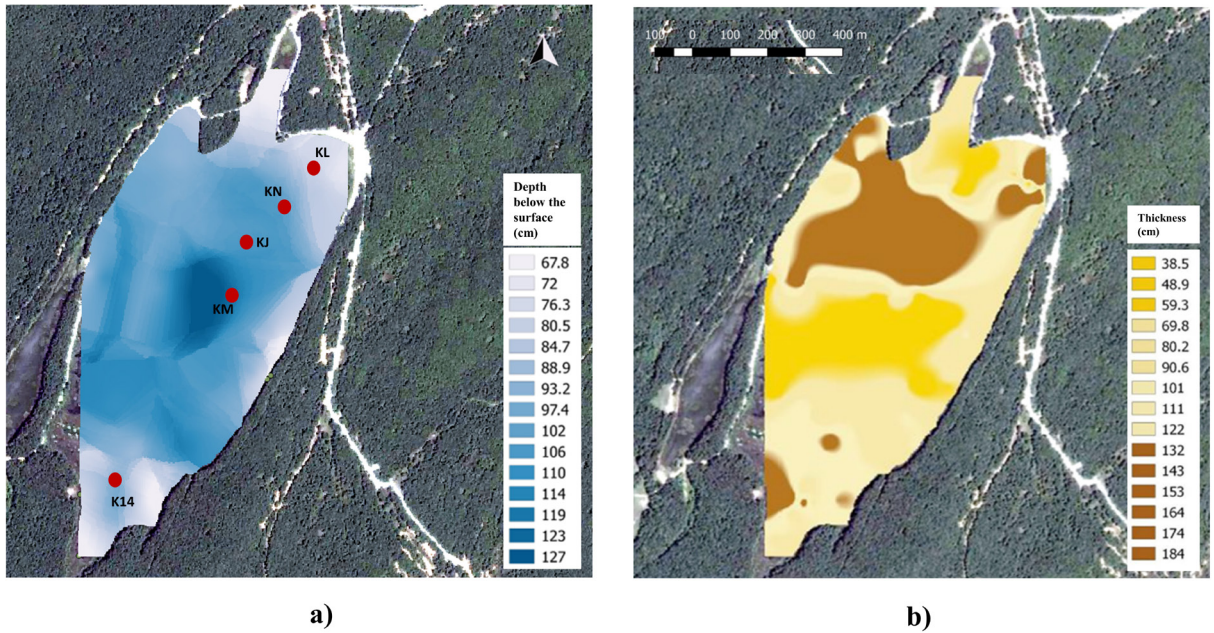
Figure 3. a) Bathymetry map of SDL, showing the location of studied cores K14, Kj, Kl, Kn, and Km which are used for various analyses (red dots), b) Sediment thickness map of the SDL.

Table 1. Location, length and stratigraphic information of cores used for the various analyses in this study.

Core number	Location Latitude/longitude	Core length (cm)	Peat unit thickness (cm)	Sand-silt-clay unit thickness (cm)
Kl	41°18'1.67"N 28°13'16.89"E	138.5	112	26.5
Kn	41°17'59.67"N 28°13'14.89"E	167	113	54
Kj	41°17'58.53"N 28°13'13.84"E	165	118	47
Km	41°17'52.61"N 28°13'6.73"E	194	146	48
K14	41°17'40.70"N 28°12'58.43"E	67	23	44

Technical University (İTU). They were stored at 4 °C in a cold room until sampling. The cores were split into two halves: one half was used for lithological description and mineral magnetic, geochemical, and radiocarbon dating analyses, while the other (archive) half was used for the nondestructive μ-X-ray fluorescence (XRF) elemental and physical property (multisensor core logger, MSCL) analyses.

2.4. AMS radiocarbon dating and age modeling
Radiocarbon dating measurements were made on total organic carbon of four samples from core Kn after acidification by accelerator mass spectrometry (AMS) at TÜBİTAK Marmara Research Centre (Table 2). The AMS radiocarbon ages were calibrated to calendar years using the OxCal 4.2 program (https://c14.arch.ox.ac.uk/oxcal.html; Bronk Ramsey and Lee, 2013). No reservoir correction was applied, assuming that there is no hard-water effect and that organic carbon in the samples are mainly of land-plant origin (for discussion, see subsection 4.1). The radiocarbon ages were used for the construction of age-depth model of core Kn with the R-studio and the script "CLAM" (Blaauw, 2010). The script creates a non-Bayesian, cubic spline age-depth model, and calculates 95 % Gaussian confidence interval around the best model.

Tablo 2. Radiocarbon dating results of samples from core Kn recovered in the SDL.

Laboratory number	Core depth (cm)	δ¹³C(‰)	Radiocarbon age (BP)	Calibrated year BP
TÜBİTAK-0384	30	−26.4 ± 2.0	4816 ± 43	5625 ± 89
TÜBİTAK-0385	72	−27.0 ± 1.7	5580 ± 41	6435 ± 71
TÜBİTAK-0309	117	−27.3 ± 0.8	7508 ± 36	8410 ± 55
TÜBİTAK-0310	122	−29.7 ± 0.7	7808 ± 36	8755 ± 99

2.5. μ-XRF elemental analysis

An ITRAX μ-XRF (X-ray fluorescence) core scanner equipped with XRF-EDS at the Core Analysis Laboratory of EMCOL was used for multielement analysis of cores Km and Kn at 0.5-mm resolution (Croudace et al. 2006; Thomson et al. 2006). A fine-focus Mo X-ray tube was used as the source. The X-ray generator was operated at 30 kV and 50 mA, and a counting time of 10 s was applied. The relative elemental abundances were recorded as counts per second (cps).

2.6. Geotek multisensor core logger (MSCL) physical properties analyses

Physical properties, including magnetic susceptibility (MS) and gamma density, were measured in five cores (Kj, Km, Kn, Kl and K14) at 2-cm resolution according to the standard procedures, using a Geotek multisensor core logger (MSCL) at the Core Analysis Laboratory of EMCOL (Weaver and Schultheis, 1990).

2.7. Environmental magnetism

Environmental magnetism is an efficient approach to investigate environmental conditions during deposition and diagenesis. It is based mainly on the redox changes of Fe^{2+} or Fe^{3+} ions hosted in iron oxides, iron oxyhydroxides, iron sulfides, or in carbonate crystal lattices (Liu et al., 2012). Magnetic susceptibility (κ_{LF}), anhysteretic remanent magnetisation (ARM), and isothermal remanent magnetization (IRM) were measured to explore the processes of formation, transportation, deposition, and postdepositional alterations of magnetic minerals. A total of 578 subsamples from ten cores were taken continuously along the cores into 6.0 cm³ plastic boxes. κ_{LF}, ARM, and IRM measurements were performed using Bartington MS2B, LDA5 Molspin AF demagnetizer and Molspin pulse magnetizer, respectively. IRM was imparted using a static peak field of 1 T and a reverse field of 300 mT (IRM_{-300mT}) to obtain Saturation IRM (SIRM) and IRM_{-300mT}, respectively. S-ratio was calculated by formula: S-ratio = $0.5 \times (1-(IRM_{-300}/SIRM))$ (Bloemendal et al, 1992). All enviromagnetic measurements were made in Yılmaz İspir Paleomagnetism Laboratory of İstanbul University-Cerrahpaşa. These magnetic parameters are widely used for discrimination of magnetic minerology,

lithological correlation between the sediment cores, and paleoenvironmental reconstuctions in lake and marine basins (Makaroğlu et al., 2018; 2020). S-ratio is used to discriminate the magnetic mineralogy; it varies between 1 and 0, depending on the predominace of low coercivity minerals (e.g., magnetite) and high coercivity minerals (e.g., hematite), respectively. κ_{LF} is roughly proportional to the concentration of ferrimagnetic and paramagnetic minerals in the samples. SIRM reflects magnetic mineral concentration if the magnetic grain size and mineralogy remain relatively constant (Liu et al., 2012). ARM and SIRM are interpreted principally in terms of variations in the overall concentration of ferrimagnetic minerals, but ARM also reflects changes in grain size distribution and the relative amounts of different ferrimagnetic minerals (Thompson and Oldfield, 1986). In this study, we used κ_{LF} mainly for core crosscorrelations, and ARM, SIRM and S-ratio for discriminating between the peat layers and the underlying sedimentary unit, and for investigating temporal paleoenvironmental changes in the lake.

3. Results

3.1. Bathymetry, morphology and sediment thickness and volume

The bathymetry map, constructed from GPR data, shows that the maximum water depth of 1.3 m is located in the central part of the lake (Figure 3a). The water depth gets shallower and reaches 60 cm near the coasts (at least up to the limit of the GPR transects).

Stratigraphic interpretation of the GPR data was based on the characteristics of the reflectors, as shown by interpretation of a sample radargram in Figure 4. The stratigraphic units defined in the radargrams were further verified by correlation with lithostratigraphic units in the cores. The results indicate that the lake is characterized by parallel-layered reflections with a sharp boundary between an upper peat unit and the underlying clastic unit (see subsection 3.2 for lithological descriptions of the cores).

The peat unit has a relatively low GPR reflectivity, with locally visible internal sedimentary bedding. Using the reflection characteristics and correlation with cores, the thickness of the peat unit was determined along each
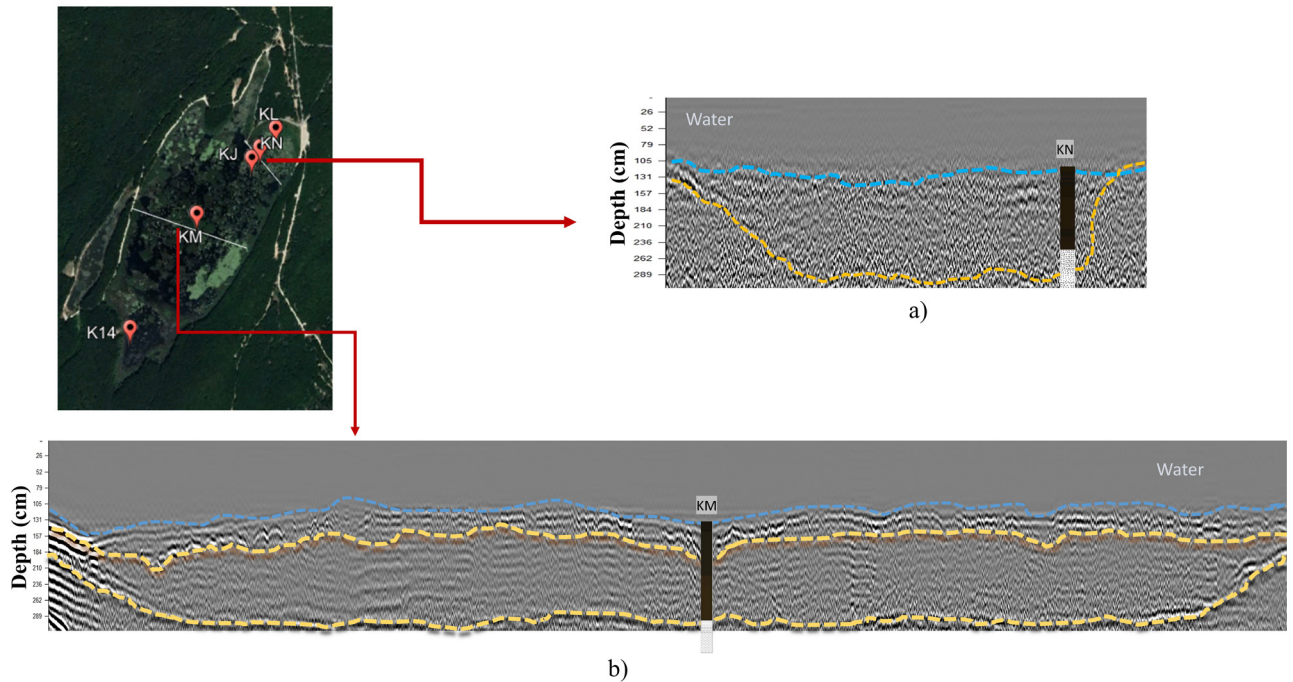
Figure 4. GPR profiles 14 and 29.

radargram, and used to construct an isopach map by utilizing ArcGIS Spatial Analyst Tool (Figure 3b). The isopach map shows that the peat thickness reaches up to 1.84 m in the lake. Greater than 1.20 m peat unit thickness is observed in a relatively large area in the north and in small patches in the south and northeast of the lake. The average peat volume is calculated as 231,896.02 m³, using ArcGIS Spatial analyst tool/ Volume 3D analyst.

3.2. Sedimentology

In the SDL cores, two lithostratigraphic units are present; an upper peat unit and a lower sand-silt-clay unit. The thickness of the upper peat unit ranges from 10 cm to 161 cm, and the thickest layer was observed in the central, western and eastern parts of the lake. It is relatively thin near the northern and southern coasts of the lake. In its upper parts, the unit consists of dark brown, very dark brown to black and locally reddish brown, slimey (watery) organic-rich mud with plant fragments (Figure 5). In some cores such as Kl, the upper part of the unit contains one or more, a few centimeters thick, light colored silty clay-rich interbeds. In its lower parts, the peat unit shows transition to very dark brown banded organic-rich mud (peat) with lesser water content. The intercalation of clay-silt-rich and relatively organic-poor beds are especially common in cores recovered from near the southern coastal areas.

The boundary between the peat unit and the underlying siliciclastic sand-silt-clay unit tends to be transitional. The transitional character is shown by an upward increase in organic carbon content and darkness of the grey color

in the upper part of the siliciclastic unit. The sand-silt-clay unit shows different vertical lithological changes in different parts of the lake. For instance, in the core Km recovered from the central part of the lake, a 10-cm-thick, organic-rich black brown clay at the top shows a gradual downward change from a 7 cm-thick dark greyish brown mud to a reddish grey silty-clayey mud (Figure 5). In core Kn, located in the NE central part, the unit consists of 8-cm thick, grey sandy silt at the base of the core, 17 cm-thick light grey, well-sorted, upward coarsening, medium-grained sand in the middle, and 29 cm-thick dark grey to brown, relatively organic-rich, sandy-silty mud on the top. In core Kj in the northeastern central part and in core Kl in the northeast of the lake, the siliciclastic unit is silty clay, and the color changes from dark grey at the top of the unit to grey near the base of the cores. In core K14 from the southern part of the lake, the unit consists of grey sandy-silty mud, which shows an upward increase in the sand content (Figure 5).

3.3. Chronostratigraphy, age-depth model, and sedimentation rates

Five selected cores have two sedimentary units: an upper peat unit and an underlying fine sand-silt-clay (siliciclastic) unit. The boundary between the two units at 113 cm core depth in core Kn is dated at 8100 ± 70 cal year BP (Table 2). According to the age-depth model, the top of the core is dated at 4250 ± 608 cal year BP (Figure 6a). Sedimentation rate in the peat unit reaches the highest values of 0.50–0.59 mm/year during 5.9–6.4 cal kyr BP interval (Figure
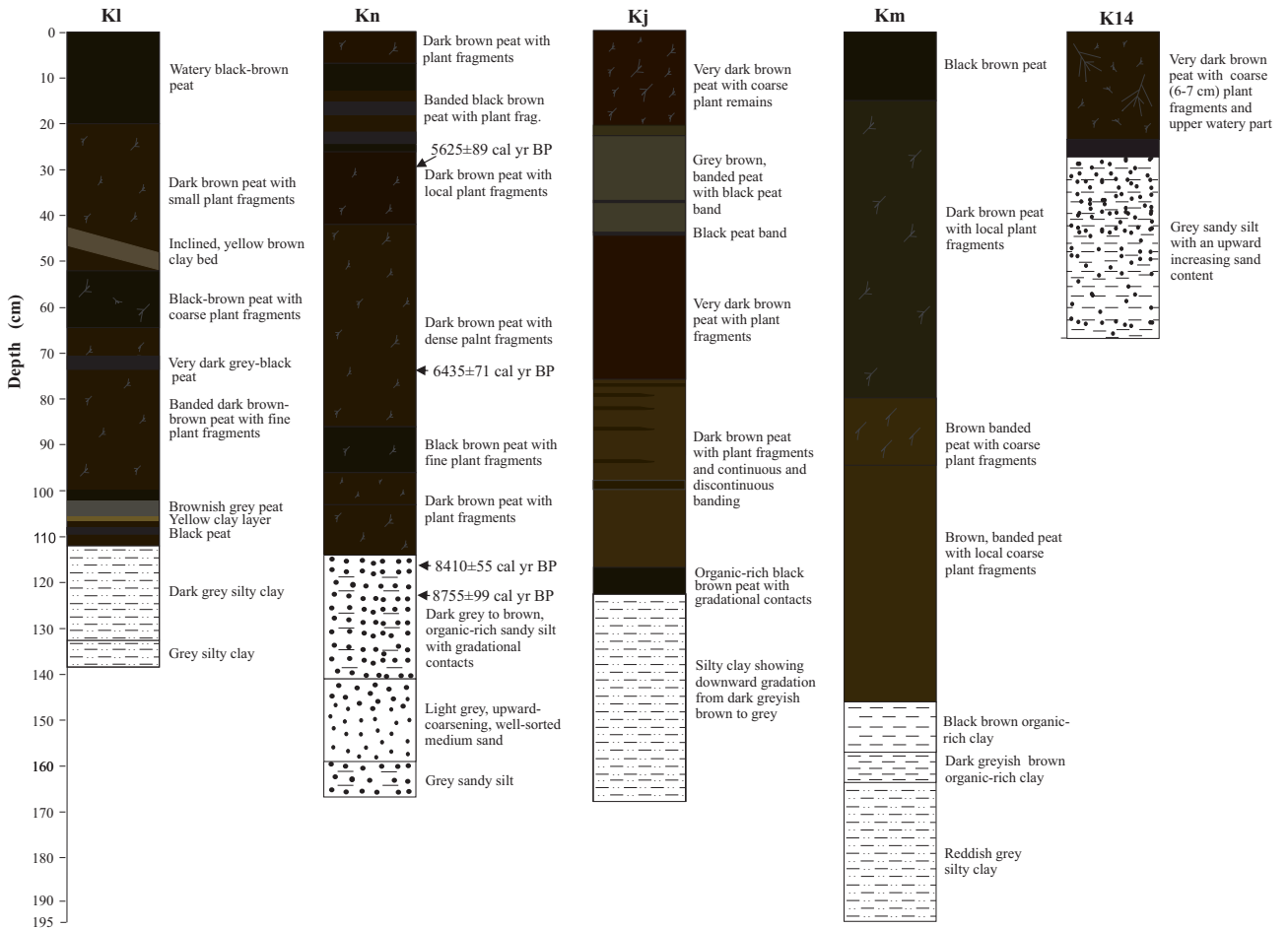
Figure 5. Lithological description of five cores along a NE-SW transect. Note the calibrated radiocarbon ages for core Kn.

6b). The rates decrease significantly upward to 0.15 mm/year at the core top and downward to 0.04 mm/year in the siliciclastic unit at bottom of the core.

3.4. Physical and magnetic properties
The MSCL gamma density profiles of the SDL cores are shown in Figure 7. The upper peat unit is characterized by low gamma density (1.60–1.85 g/cc), whereas the underlying siliciclastic (sand-clay-silt) unit has variable density values between 1.45 g/cc and 2.3 g/cc. Relatively high density values for the lower unit are observed in cores Kn and Km (e.g., Kl and Kn). The upper part of the peat unit contains some positive excursions in density in cores Kl, Kj and K14, which correspond to silty mud intercalations.

Magnetic susceptibility ($κ_{LF}$) values commonly increase downward from the peat unit to the siliciclastic unit (Figure 7). This increase in $κ_{LF}$ is especially pronounced at the boundary between the two units in cores Kj, Km, Kl and Ke. The SIRM and ARM profiles of the SDL cores clearly define the lithological boundary between the peat and siliciclastic units, with relatively uniform, low values of magnetic parameters in the upper unit, and high and relatively variable values in the lower unit (Figure 8). SIRM profile in the peat unit in core Kn shows some positive excursions in the upper part of the unit corresponding to the clay-silt interbeds. S-ratio values in the siliciclastic unit in core Km is also higher and more uniform than that of the peat unit.

3.5. Geochemistry
The organic carbon content of the peat unit ranges between 17 wt%, and 56 wt%, with an average of 39.5 wt%, and an average of the atomic C/N ratio of 15.7 (Karaöz et al., 2020). The peat unit and the underlying sand-silt-clay unit do not contain any inorganic carbon (i.e. carbonate minerals).

K, Ti, Zr, Fe, and Mn are significantly more enriched in the sand-silt-clay unit compared with the peat unit, whereas µ-XRF Br is relatively higher in the peat unit (Figure 9). µ-XRF K, Ti and Zr profiles show some positive excursions in the peat unit in the upper 5–20 cm of cores Kn and Km (Figure 9). In core Km, µ-XRF Fe shows a negative excursion in the interval between 1.62 and 1.68
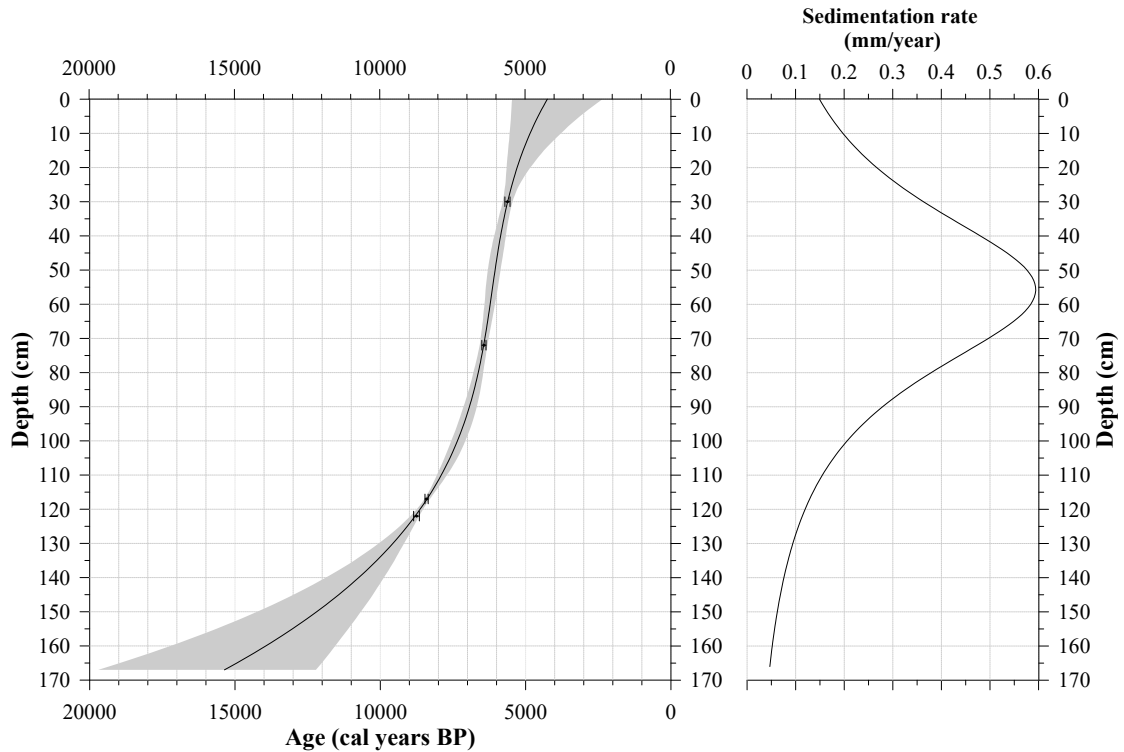
Figure 6. (a) Age-depth model of core Kn, (b) Sedimentation rate profile of core Kn.

m. In core Kn, μ-XRF K is relatively enriched in the 1.30–1.55 m interval, while μ-XRF Fe, Ti and Zr are high in the upper part of the sand-silt-clay unit and in the basal part of the core (Figure 9). The redox-sensitive μ-XRF Mn has very low counts in the peat unit, except for a slight enrichment in the upper parts.

4. Discussion

4.1. Radiocarbon age of the lake
The age-depth model of core Kn indicates an age of 4250 ± 608 cal year BP for the top of the core (Figure 6). This may be due to either hard-water effect (radiocarbon reservoir age) or removal of recent sediments (peat).

Several lines of evidence suggest that there is no hard water (i.e. radiocarbon reservoir) effect in the SDL, and the calibration of the radiocarbon ages to calendar years does not require a reservoir age correction. First, the lake's drainage area is totally situated on the siliciclastic Ergene Formation, which does not include any carbonate minerals. Similarly, the peat unit is devoid of carbonate minerals mainly because of the acidity of its interstitial waters (pH: 4.09–6.88 (Karaöz et al., 2020). Second, the high average C/N values (average of all cores: 15.7; average of core Kn: 16.6; Karaöz et al., 2020) and light $\delta^{13}C$ values (−29.7 to −26.4 ‰; Table 2) of the organic matter in the lake suggest that organic matter is mainly of land plant origin (Hedges and Oades, 1997; Goñi et al., 2003)

(i.e. common reed, *Phragmites* sp.), and hence, the carbon source is almost totally of the atmospheric CO_2. Third, although the SDL is presently a closed lake, it was most likely a small open lake with an outflow over the shallow sill in its south during the pluvial periods. The last time such an outflow occurred during the year 1990 was by human interference, when the lake was emptied through the sill. Therefore, we argue that the absence of the 4.25 kyr sedimentary record for the core Kn is mainly due to the removal of peat from the lake during 1990–1995 (Personal communication with residents of the Danamandıra Village). In the core sections, we consider that the onset of lake sedimentation started with deposition of organic-rich silty mud, below the peat unit (see discussion in subsection 4.2 below). The basal boundary of the first organic-rich sandy silt bed in the radiocarbon-dated core Kn is at 141 cm, which corresponds to the age of 10.88 ± 0.61 cal kyr BP, representing the starting age of the lake.

4.2. Depositional facies and sedimentation history
Morphological analysis of the Danamandıra area indicates that the SDL formed in a shallow depression in the fluvial channel connecting the North Danamandıra Lake to the Süpürge Stream (Figure 1). This conclusion is further supported by variations in the lithology (i.e. grain size) and physical properties (i.e. density and magnetic susceptibility) of the sand-silt-clay unit in the different SDL cores, which are the common characteristics of the fluvial
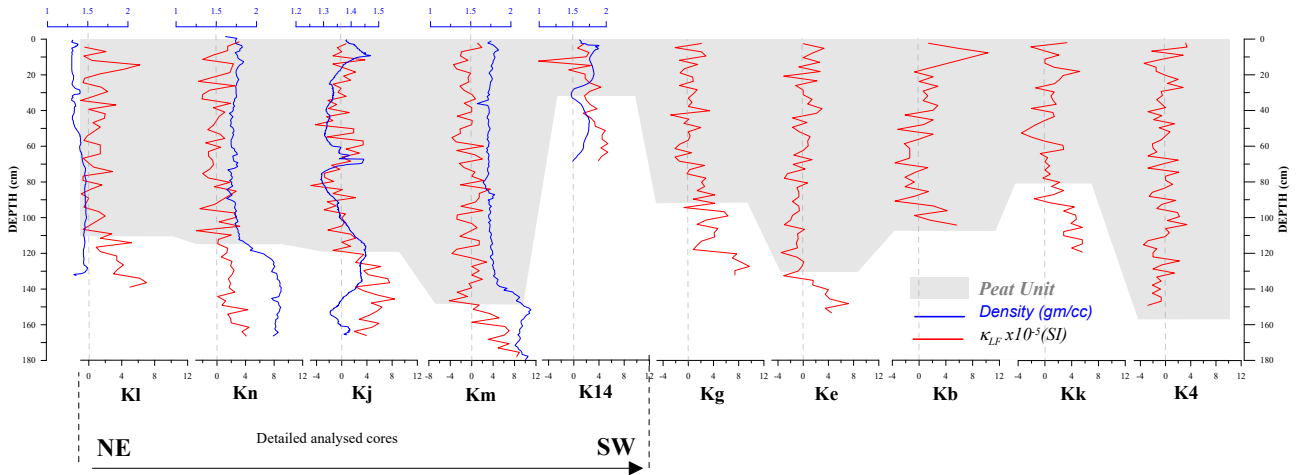
Figure 7. Correlation of ten cores taken from the different location in the SDL, using magnetic susceptibility (κ$_{LF}$) and gamma density. For location of the cores, see Figure 3a.
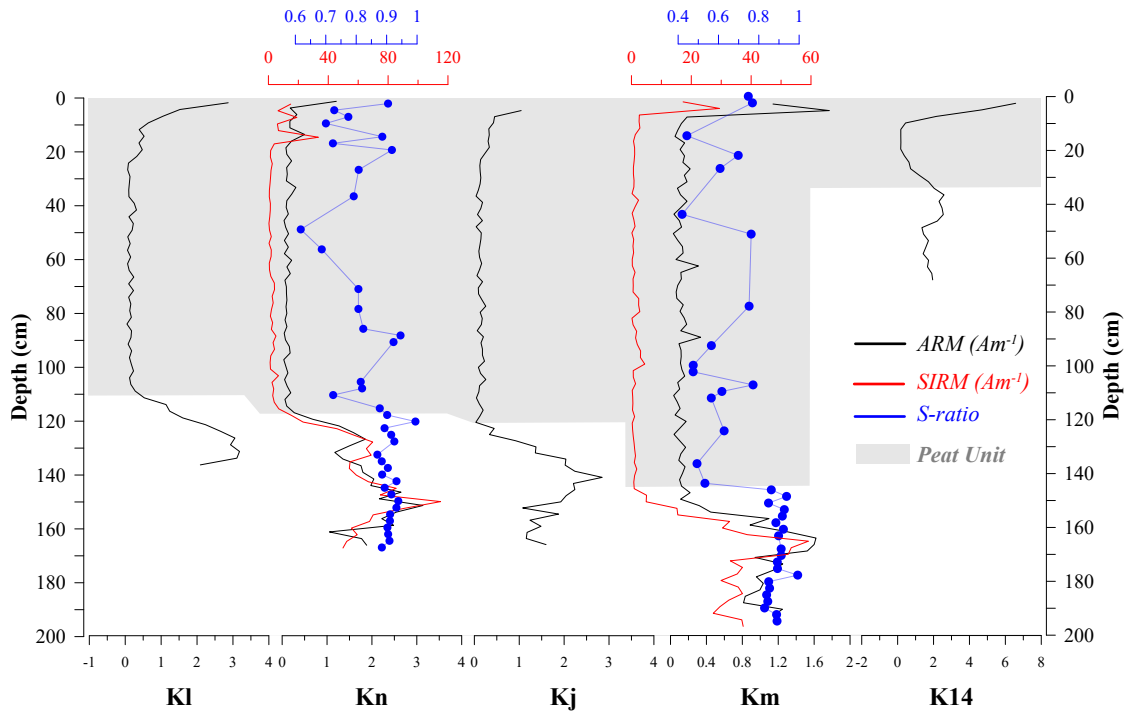

Figure 8. Mineral magnetic properties of sediment cores from SDL. ARM = Anhisteretic remanent magnetisation. SIRM = Saturation isothermal magnetisation.

systems. Such systems are characterized by rapid temporal and spatial variability of facies which develop by processes of channel migration over a floodplain and overbank flow, and are highly sensitive to uplift, subsidence and climatic changes (e.g., Miall, 2006).

The lithology of the siliciclastic unit is very similar to that of the Upper Miocene Ergene formation described from the area by Yurtsever and Çağlayan (2002). Hence, the sand-silt-clay unit may represent the reworked siliciclastic material of the Ergene Formation, which was deposited under fluvial-lacustrine conditions, starting at 10.88 ± 0.61 cal kyr BP. This age approximately corresponds to the onset of the Holocene warm period during which the global average temperature increased by 3–6 °C (e.g., Davis et al., 2003; Kaufman, et al., 2004). This period is characterized in NW Anatolia by relatively warm and humid conditions, as evidenced by pollen studies in the Sea of Marmara and in the İznik and Manyas lakes
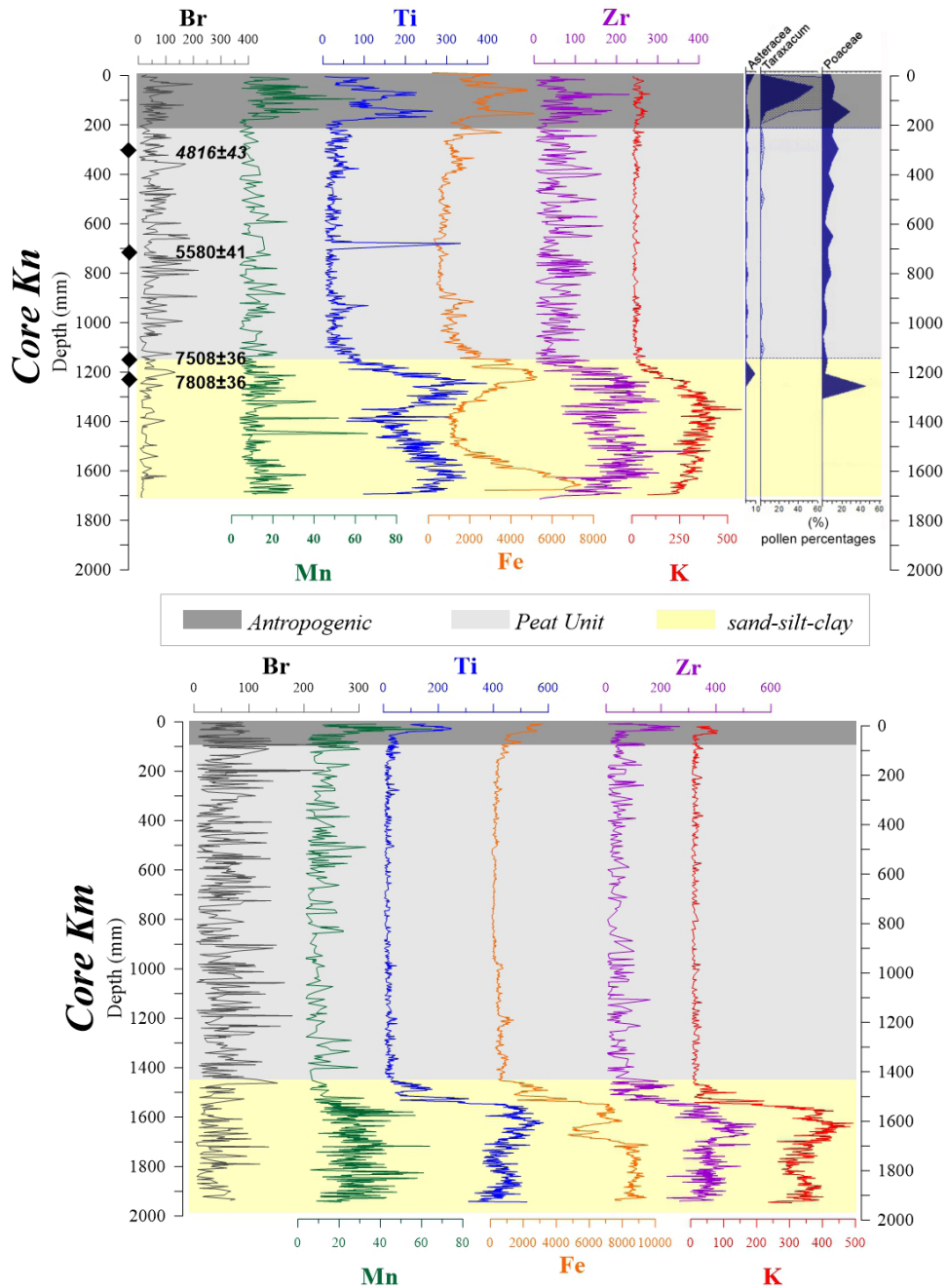
Figure 9. XRF-core scanner analysis of SDL cores Kn and Km and pollen percentage chart for core Kn. Diamonds show location of radiocarbon dated samples, with calibrated ages (year BP), in core Kn.

(Mudie et al., 2002; Caner and Algan, 2002; Leroy et al., 2002; Valsecchi et al., 2012; Miebach et al., 2016). Mineral magnetic properties and in particular high SIRM values in the sand-silt-clay unit indicate relatively high contents of ferrimagnetic minerals delivered as part of the detrital input under oxic water-column conditions (Channell and Hawthorne, 1990; Rowan et al., 2009). During this humid period, the SDL level was likely high, and the lake was outflowing via its southern natural outlet.

The upper part of the siliciclastic unit shows an upward increase in organic carbon and darkness in grey color, and was deposited under lacustrine conditions with moderate organic production. In core Kn, K enrichment in the 1.25–1.65 m core interval in the unit suggests increased illitic clay content from ca. 14.9 ± 2.46 to 9.07 ± 0.13 cal kyr BP, while Ti, Zr and Fe enrichments occur in two peaks corresponding to ca. 13.03 ± 1.31 kyr and 9.57 ± 0.25 cal year BP and indicate lithophile element enrichments

related to high fluvial activity during these periods. The boundary between the siliciclastic unit and the overlying peat unit is placed at the stratigraphic level where a sharp upward drop in the physical properties (magnetic susceptibility, remanent magnetic properties and density) and lithophile elements profiles are observed (Figures 7–9). In core Kn, the boundary occurs at 113 cm, which corresponds to an age of 8.1 ± 0.07 cal kyr BP that marks the onset of peat deposition.

Low density, magnetic susceptibility, low lithophile elements (K, Fe, Ti and Zr) µ-XRF counts and in part uniformly low values of SIRM and ARM in the peat unit show considerably reduced detrital input in the SDL during its deposition, compared to that during the detrital sand-silt-clay unit. However, the lithophile elements show some enrichment in the upper 10–25 cm of the peat unit in cores Kn and Km, indicating high detrital input in the lake during 4.8–5.4 cal kyr interval, which may be due to increased human activities around the lake. Archaeological, geochemical and palynological studies show that detrital events related to global climatic changes and anthropogenic activities were common in the Marmara region as well as in western Anatolia and Mediterranean region during the Early Bronze Age (e.g., Fidan et al., 2005; Ülgen et al., 2012; Vella et al., 2019; Mayoral et al., 2020). This Early Bronze Age human influence in the study area, such as forest clearance and farming, likely resulted in increased erosion rates, and is supported by rise in *Taraxacum*, Asteraceae and Poaceae pollen percentages in the topmost 25 cm of core Kn (Figure 9).

Bromine is usually enriched in marine sedimentary organic matter (Ziegler et al., 2008). In the peat unit of the SDL, it is only slightly enriched relative to the underlying sand-silt-clay unit, supporting the fact that the organic matter of the Danamandıra peat unit is of lacustrine-terrestrial origin, with no marine influence (Figure 9). As discussed in the previous section, the high C/N ratios (average: 16.6) and low δ¹³C values (–29.7 to –26.4 ‰) strongly suggest that organic matter of the peat consists predominantly of terrestrial plant origin. This conclusion is supported by the frequent occurrence of *Phragmites* sp. and *Carex* sp. plant fragments in the peat unit. The SDL peat appears to have formed as a swamp peat in the topographic depression of a fluvial channel during the last 8.01 ± 0.07 cal kyr BP. Its maximum development with high organic production and sedimentation rates took place under warm and wet conditions during 5.9–6.4 cal kyr BP. The onset of this peak peat formation during the middle Holocene coincides with the deposition of an organic-rich sediment unit (sapropel) in the Sea of Marmara under similar climate conditions (Çağatay et al., 1999; 2015). The SDL peat formation took place under subbottom anoxic conditions as indicated by the very low µ-XRF counts of

Mn, low SIRM and ARM values and a strong H_2S smell. Mn is a redox sensitive element that is depleted in anoxic sediments (Calvert and Pedersen, 1993; Thomson et al., 1995; Çağatay et al., 1999). Its enrichment, together with Fe, in the uppermost part of peat unit is due to both surficial oxic conditions and the detrital siliciclastic input. The low SIRM and ARM values of the peat unit are mainly due to the relatively low siliciclastic input as well as the sulphidic diagenetic changes under reducing conditions during the peat deposition.

In summary, after the onset of lacustrine conditions in the fluvial channel depression at 10.88 ± 0.61 cal kyr BP, the SDL gradually became a eutrophic lake starting at 8.1 ± 0.06 cal kyr BP during the early Holocene pluvial period. It was soon colonized by plants (mainly *Phragmites* sp., *Carex* sp., *Juncus* sp., *Iris* sp. and *Nymphea* sp.), which lead to peat mire development and peat formation under anoxic conditions.

5. Conclusion

The SDL formed in a shallow depression of a fluvial channel at ca 10.88 ± 0.61 cal kyr BP. It became a eutrophic lake during the early Holocene warm period, and has gradually developed into a swampy peatland at 8.1 ± 0.06 cal kyr BP. The high C/N and low δ¹³C values shows that the organic matter of the peat unit is of terrestrial-lacustrine origin. Redox sensitive elements (e.g., Mn) distributions and mineral magnetic properties indicate that the peat unit accumulated under anoxic conditions below a thin oxic surficial layer. The human influence in the area started at 5.4 cal kyr BP, as indicated by increased erosion with high siliciclastic input and increase in the *Taraxacum*, Asteraceae and Poaceae pollen percentages.

Contribution of authors

ÖM: Leading manuscript, conceptualization, visualisation, data interpretation, mineral magnetic analysis, discussion

and writing original draft, reviewing, and editing. **MK:** Conceptualization, GPR data acquisition and processing, discussion and writing. **NKK:** Polen data acquisition and processing. **DA**: Fieldwork, coring, sampling, XRF analysis. **AG**: Fieldwork. **YD**: Polen analysis. **NY**: Age model.

AS: Topography map. **DŞA**: Field work. **MÖK:** Project administration, field work. **MNÇ:** Conceptualization, data interpretation, formal discussion, geochemical analysis, reviewing, and editing.

References

Acar TO, Durak SG, Tüfekci N (2017). Effects of fulvic acid and ferric hydroxide on removal of Fe2+ and Mn2+ by oxidation and aerated/submerged ultrafiltration membrane system. Water Science & Technology: Water Supply 17: 1712-1721.

Albayrak E, Ozulug O (2016). Danamandıra Gölü (Silivri-İstanbul) Bentik Makro omurgasızları. Turkish Journal of Aquatic Sciences 31 (1): 51-58. doi: 10.18864/tjas201606.

Blaauw M (2010). Methods and code for "classical" age-modeling of radiocarbon sequences.

Quaternary Geochronology 5 (5): 512-518. doi: 10.1016/j.quageo.2010.01.002

Bloemendal J, King JW, Hall FR, Doh SH (1992). Rock magnetism of late Neogene 405 and Pleistocene deep-sea sediments: Relationship to sediment source, 406 diagenetic processes, and sediment lithology. Journal of Geophysical Research 97: 4361–4375.

Bronk Ramsey C, Lee S (2013). Recent and Planned Developments of the Program OxCal. Radiocarbon 55 (2-3): 720–730.

Butler KE (2009). Trends in waterborne electrical and EM induction methods for high resolution sub-bottom imaging. Near Surface Geophysics 7: 241-246.

Calvert SE, Pedersen TF (1993). Geochemistry of Recent oxic and anoxic sediments: Implications for the geological record. Marine Geology, 113: 67-88.

Caner H, Algan O (2002). Palynology of sapropelic layers from the Marmara Sea. Marine Geology 190: 35–46.

Channell JET, Hawthorne T (1990). Progressive dissolution of titanomagnetites at ODP Site 653 (Tyrrhenian Sea). Earth and Planetary Science Letters 96: 469–480. doi: 10.1016/0012-821X(90)90021-O

Crapper M (2020). The valens aqueduct of constantinople: hydrology and hydraulics. Water History 12: 427–448. doi: 10.1007/s12685-020-00254-4

Croudace W, Rindby A, Rothwell RG (2006). ITRAX: description and evaluation of a new multi-function X-ray core scanner. In: Rothwell, R.G. (Ed.), New Techniques in Sediment Core Analysis 267: 51-63. Geological Society, London Special, Publication.

Çağatay MN, Algan O, Sakınç M, Eastoe C, Egesel L et al. (1999). A mid-late Holocene sapropelic sediment unit from the Southern Marmara shelf and its Paleoenvironmental significance. Quaternary Science Reviews 18: 531-540.

Çağatay MN, Wulf S, Guichard F, Özmaral A, Henry P et al. (2015). Tephra record from the Sea of Marmara for the last 71 ka and its paleoceanographic implications. Marine Geology 361: 96-110.

Çolak A H, Günay T (2011). Turbalıklar (Mire/Peatland-Moore). İstanbul: T.C. Orman ve Su İşleri Bakanlığı, Batı Karadeniz Ormancılık Araştırma Enstitüsü Müdürlüğü-Bolu, Çeşitli Yayınlar Serisi No.7 Müdürlük Yayını No.25 (in Turkish). ISBN: 978-605-393-115-7.

Davis BAS, Brewer S, Stevenson AC, Guiot J (2003). The temperature of Europe during the Holocene reconstructed from pollen data. Quaternary Science Reviews 22 (15–17): 1701–16. doi: 10.1016/S0277-3791(03)00173-2.

Doğan ÖS (2011). Silivri'de turizmin gelişmesi: sorunlar ve çözüm önerileri. *Eastern* Geographical Review 16 (25): 89-102.

EU Copernicus Land Monitoring Service, (2020). Accessed 10.01.2021.< https://www.copernicus.eu/en>

Fidan E, Sarı D, Türkteki M (2015). An Overview of the Western Anatolian Early Bronze Age. European Journal of Archaeology 18 (1): 60–89.

Goñi M A, Teixeira MJ, Perkey DW (2003). Sources and distribution of organic matter in a river-dominated estuary (Winyah Bay, SC, USA). Estuarine, Coastal and Shelf Science 57: 1023–1048. doi: 10.1016/S0272-7714(03)00008-8

Hedges JI, Oades JM (1997). Comparative organic geochemistries of soils and marine sediments. Organic Geochemistry 27: 319–361. doi: 10.1016/S0146-6380(97) 00056-9

Justen H, Clarke D (2002). Wise Use of Mires and Peatlands - Background and Principles Including a Framework for Decision-Making. International Mire Conservation Group and International Peat Society, 304pp. ISBN 951-97744-8-3.

Karaöz MÖ, Tutar A, Horuz A, Karlıoğlu Kılıç N, Makaroğlu M et al. (2020). Formation processes of living (main) peats of the Marmara Region, using pollen and humic-matter structural analyses. TÜBİTAK Project (117O627) Report (in Turkish with English abstract).

Kaufman, DS, Ager TA, Anderson NJ, Andersond PM, Andrews JT et al. (2004). Holocene thermal maximum in the western Arctic (0–180 W). Quaternary Science Reviews 23 (5–6): 529–560.

Leroy S, Kazancı N, İleri Ö, Kibar M, Emre Ö et al. (2002). Abrupt environmental changes within a late Holocene south of the Marmara Sea (Lake Manyas, N-W Turkey): possible links with seismic events. Marine Geology 190: 531–552.

Liu Q, Roberts AP, Larrasoaña JC, Banerjee SK., Guyodo Y et al. (2012), Environmental magnetism: Principles and applications. Reviews of Geophysics 50, RG4002, doi: 10.1029/2012RG000393

Makaroğlu Ö, Çağatay MN, Nowaczyk NR, Pesonen LJ, Orbay N (2018). Discrimination of Holocene tephra units in Lake Van using mineral magnetic analysis. Quaternary International 486: 44-56. doi: 10.1016/j.quaint.2018.03.012

Makaroğlu Ö, Nowaczyk NR, Eriş K, Çağatay MN (2020). High-resolution palaeomagnetic record from Sea of Marmara sediments for the last 70 ka. Geophysical Journal International 222 (3): 2024–2039. doi: 10.1093/gji/ggaa281

Mayoral A, Berger JF, Peiry JL, Ledger P, Miras Y (2020). Five millennia of human environment interactions reconstructed from pedosedimentary archives of the Lac du Puy Wetland (Corent, Fr.). CATENA Elsevier 195: 104908. doi: 10.1016/j.catena.2020.104908

Miall AD (2006). The Geology of Fluvial Deposits Sedimentary Facies, Basin Analysis, and Petroleum Geology. Springer-Verlag Berlin Heidelberg GmbH. SBN 978-3-642-08211-5. doi: 10.1007/978-3-662-03237-4.

Miebach A, Niestrath P, Roeser P, Litt T (2016). Impacts of climate and humans on the vegetation in northwestern Turkey: palynological insights from Lake Iznik since the Last Glacial. Climate of the Past 12: 575–593.

Mudie PJ, Rochon A, Aksu AE (2002). Pollen stratigraphy of Late Quaternary cores from Marmara Sea: land–sea correlation and paleoclimatic history. Marine Geology 190: 233–260.

Neal A (2004). Ground Penetrating Radar and Its Use in Sedimentology: Principle, Problem and Progress. Earth Science Reviews 66: 261-330. doi: 10.1016/j.earscirev.2004.01.004

Okay AI, Özcan E, Hakyemez A, Siyako M, Sunal G et al. (2019). The Thrace Basin and the Black Sea: the Eocene - Oligocene connection. Geological Magazine 156: 39-61.

Quézel P, Médail F (2003). Ecologie et biogéographie des forêts du bassin méditerranéen. Elsevier, Paris (571 pp.).

Republic of Türkiye Ministry of Forestry and Water Affairs (2012). Bakanlık raporları, 2012 (in Turkish).

Rowan CJ, Roberts AP, Broadbent T (2009). Reductive diagenesis, magnetite dissolution, greigite growth and paleomagnetic smoothing in marine sediments: A new view. Earth and Planetary Science Letters 277: 223–235. doi: 10.1016/j.epsl.2008.10.016

Ruggeri F (2018). Engineering the Byzantine Water Supply of Constantinople: mapping, hydrology and hydraulics of the long aqueducts outside the City. The University of Edinburgh, Edinburg.

Sambuelli L, Bava S (2012). Case study: A GPR survey on a morainic lake in northern Italy for bathymetry, water volume and sediment characterization. Journal of Applied Geophysics 81: 48-56. doi: 10.1016/j.jappgeo.2011.09.016

Sevindik Ongun T, Gönülol A, Önem B, Tunca H, Arabacı S (2015). Thirty new records for Turkish freshwater algal flora from Danamandıra Ponds (Silivri, İstanbul) and North Mollaköy Lake (Sakarya). Biological Diversity and Conservation 8 (2): 4-15.

Ülgen UB, Franz SO, Biltekin D, Çağatay MN, Roeser PA et al. (2012). Climatic and environmental evolution of Lake Iznik (NW Turkey) over the last ~4700 years. Quaternary International 274: 88-101.

Tanneberger F, Tegetmeyer C, Busse S, Barthelmes A, Shumka S et al. (2017). The peatland map of Europe. Mires and Peat, 19 (Art.22), pp. 1-17. doi: 10.19189/MaP.2016.OMB.264

Thompson R, Oldfield F (1986). Environmental Magnetism, Allen and Unwin (Publishers) Ltd, 40 Museum St., London, 0-04-538003-1.

Thomson J, Croudace IW, Rothwell RG (2006). In: Rothwell R.G. (Ed.), A Geochemical Application of the ITRAX Scanner to a Sediment Core Containing Eastern Mediterranean Sapropel Units. New Techniques in Sediment Core Analysis. vol. 267. Geological Society, London, Special Publications.

Thomson J, Higgs NC, Wilson TRS, Croudace IW, De Lange GJ et al. (1995). Redistribution and geochemical behaviour of redoxsensitive elements around S1, the most recent eastern Mediterranean sapropel. Geochimica et Cosmochimica Acta 59: 3487-3501.

US/Japan ASTER Science Team (2019). ASTER Global Digital Elevation Model V003 (dataset). NASA EOSDIS Land Processes DAAC. doi: 10.5067/ASTER/ASTGTM.003

Valsecchi V, Sánchez-Goñi MF, Londeix L (2012). Vegetation dynamics in the Northeastern Mediterranean region during the past 23 000 yr: insights from a new pollen record from the Sea of Marmara. Climate of Past 8: 1941–1956.

Vella MA, Andrieu Ponel V, Cesari J, Leandri F, Pêche-Quilichini K et al. (2019). Early impact of agropastoral activities and climate on the littoral landscape of Corsica since mid-Holocene. PLoS ONE 14 (12): 0226358. doi: 10.1371/journal.pone.0226358

Yılmaz Y, Gökaşan E, Erbay AY (2009). Morphotectonic development of the Marmara region. Tectonophysics. doi: 10.1016/j.tecto.2009.05.012

Yurtsever A, Çağlayan A (2002). Geological maps of Turkey, 1. 100 000 scale, Istanbul F21 and G21 sheet and explanatory text. Maden Tetkik ve Arama Genel Müdürlüğü, Ankara, 30 pp.

Weaver PPE, Schultheis PJ (1990). Current methods for obtaininig, logging and splitting marine sediment cores. Marine Geophysical Research 12: 85-100.

Ziegler M, Jilbert T, de Lange GJ, Lourens LJ, Reichart GJ (2008). Bromine counts from XRF scanning as an estimate of the marine organic carbon content of sediment cores. Geochemistry, Geophysics, Geosystems, 9: Q05009. doi: 10.1029/2007GC001932